


Collective Resonances of a Chain of Coupled Phononic Microresonators

Ting-Ting Wang,^{1,2} Sylwester Bargiel,² Franck Lardet-Vieudrin,² Yan-Feng Wang,^{3,*}
Yue-Sheng Wang,^{1,3} and Vincent Laude^{2,†}

¹*Institute of Engineering Mechanics, Beijing Jiaotong University, 100044 Beijing, China*

²*Institut FEMTO-ST, Université Bourgogne Franche-Comté and CNRS, 25030 Besançon, France*

³*School of Mechanical Engineering, Tianjin University, 300350 Tianjin, China*

 (Received 28 September 2019; revised manuscript received 20 November 2019; published 14 January 2020)

We study experimentally a chain of defect resonators in a phononic crystal slab and observe its collective resonances at ultrasonic frequencies of a few megahertz. A phononic crystal of cross holes is fabricated in a thin fused-silica plate by femtosecond-laser writing followed by KOH etching. A chain of 17 coupled resonators is defined with no definite spatial periodicity but similar coupling strength between nearest-neighbor resonators. The full phononic band gap ensures that only evanescent waves in the crystal can tunnel between adjacent resonators in the plane. The resulting evanescent-coupling strength decreases exponentially with distance. Collective resonances are excited by a frequency-driven piezoelectric vibrator attached at one end of the chain and imaged along the chain with a laser Doppler vibrometer. A discrete spectrum of resonances is observed and explained by a model representing the chain as a phononic polymer. The theoretical analysis is supported by finite-element simulations that agree well with experimental results. Chains of evanescently coupled microresonators forming phononic polymers could find applications in ultrasonic sensing, for implementation in topological phononics, and for the design of optomechanical resonator chains.

DOI: [10.1103/PhysRevApplied.13.014022](https://doi.org/10.1103/PhysRevApplied.13.014022)

I. INTRODUCTION

Over the past two decades, there has been much effort to achieve control of waves propagating within phononic or sonic crystals exhibiting elastic or acoustic band gaps [1]. The propagation of waves is completely forbidden in band gaps [2]. Even though there are no waves propagating inside a band gap of a perfect crystal, evanescent waves still exist [3]. Besides explaining complex solutions in the dispersion relation of homogeneous media and crystals [4], evanescent waves also provide a coupling mechanism for the vibrations of periodic chains of masses connected by a spring [5,6] or of coupled-resonator waveguides [7,8]. Strong confinement and localization of waves can indeed be achieved at the frequencies in the complete phononic band gap [9–11]. When the periodicity of the perfect crystal is broken, for instance, by changing the geometry of the unit cell or the material properties, point and line defects can form cavities and waveguides, respectively [12,13].

Waveguides composed of linear chains of coupled resonators in a crystal were first proposed in the field of photonics [14]. These coupled-resonator waveguides can be designed with use of photonic crystal defect cavities

or microring resonators [15], and can have applications to slow light [16], in light storage [17], in sensing [18], and in light capture [19]. Dielectric coupled-resonator waveguides also parallel plasmonic waveguides composed of periodically distributed metal nanoparticules [20]. Coupled-resonator waveguides have been extended to the field of phononic crystals. Khelif *et al.* [21] demonstrated experimentally the guiding and the bending of acoustic waves in highly confined waveguides. Hatanaka *et al.* [22] developed a phonon waveguide using a one-dimensional array of suspended membranes and demonstrated that it could support and guide mechanical vibrations by nanoelectromechanical systems. Wang *et al.* [23] investigated experimentally Lamb-wave propagation in coupled-resonator elastic waveguides formed by a chain of cavities in a two-dimensional phononic crystal slab with cross holes. They also investigated the transmission properties of coupled-resonator acoustoelastic waveguides formed by a chain of cavities with water, such as multiply-90°-bent waveguides or wave splitters [24].

Defects in a phononic crystal have long been known to introduce localized states of vibration [25]. They have been proposed to filter the transmission through a crystal sample [26] or to alter the transmission along a waveguide [27]. In general, the defects used were small and chosen to possess well-defined isolated resonance frequencies.

*wangyanfeng@tju.edu.cn

†vincent.laude@femto-st.fr

An additional condition of periodicity at the level of a supercell is generally imposed to guarantee that the dispersion can be obtained numerically via the computation of phononic band structures. In this paper, we instead examine an extended and nonperiodic defect in a phononic crystal, based on the coupled-resonator concept, that possesses a discrete spectrum of closely spaced resonances. Coupling between adjacent resonators is not limited to straight lines or to privileged crystallographic directions. Instead, evanescent coupling inside a complete band gap is omnidirectional and decreases exponentially away from a resonator. Hence, it provides an adequate platform to implement nearest-neighbor coupling within an aperiodic chain of finite length, without the additional propagation phases that would result from attaching the resonators to a propagation medium or a surface [28,29]. Interaction between adjacent resonators is reminiscent of the chemical bonds of molecular polymers. Thus, the chain of resonators is loosely termed a “phononic polymer” in this work and it is understood that it can be deformed rather freely in the plane.

In the following, we specifically consider a chain of coupled resonators fabricated in a phononic crystal slab in fused silica that can be conveniently manufactured at the microscale. The phononic crystal slab of cross holes possesses a wide complete band gap extending from 1.5 to 4 MHz. The chain is formed by our distributing resonators along an aperiodic path but respecting an equal-coupling scheme. Collective modes of vibration of the chain are imaged with a laser vibrometer. A fine spectrum of resonances involving the motion of all resonators at once is observed. Finally, a theoretical model is proposed to explain the frequency response and to predict the discrete spectrum of resonance frequencies.

II. METHODS

Recently, femtosecond-laser-assisted wet etching has been demonstrated as a powerful mask-free micromachining method, allowing fabrication of various three-dimensional (3D) microstructures in fused silica ($a\text{-SiO}_2$) and other glass materials with high spatial precision [30]. This method is well suited for the fabrication of phononic crystal resonators due to the high selectivity of etching of glass materials in KOH, resulting in high-aspect-ratio structures with well-defined and smooth vertical sidewalls. In this work, the process parameters are adjusted to produce a significant increase in the etch rate of irradiated silica (typically 200 in 10M KOH at 80 °C). The increased etch rate can be explained by laser-induced stress generation, which is responsible for weakened chemical bonds (and hence bond-angle variations) in the SiO_2 matrix [31]. Moreover, with increasing number of laser pulses, stress builds up and a porous structure is created that can be penetrated much faster by the etchant.

The chain of coupled resonators shown in Fig. 1 is manufactured in a fused-silica plate. The sample size is 26 mm \times 20 mm \times 500 μm . A square lattice of cross holes, with lattice constant $a = 714 \mu\text{m}$, is etched in the plate by use of a 3D laser system (FEMTOprint model f100 aHEAD Enhanced) equipped with a 5-W femtosecond laser operating at $\lambda = 1030 \text{ nm}$. The overall fabrication process is a direct writing method (i.e., without a mask) and is composed of three main steps. The process flow is shown in Fig. 1(a). First, a laser-machining process is programmed in three dimensions by use of dedicated software (ALPHACAM), which results in the generation of a machining code file. Next, the fused-silica substrate is scanned by the focused laser beam, according to the program, and the material is exposed to low-energy femtosecond pulses that increase locally the etching rate. Only a very thin contour (2–2.5 μm wide) of each cross hole is exposed through the whole substrate thickness in sequential order. In the final step, the thin walls of exposed silica (aspect ratio approximately 80) are double-side etched in a 10M KOH solution at 80 °C. The total etching time is 3 h (etch rate approximately 2.2 $\mu\text{m}/\text{min}$), resulting in release of silica cross blocks into the etchant. Ultrasonic vibrations are activated periodically during etching to enhance penetration of KOH through the high-aspect structure and to stabilize the etching rate. The scanning-electron-microscope image of a cross hole (measured with Quanta 450W scanning electron microscope) in Fig. 1(b) allows us to verify the smoothness of the walls after etching. Fabrication errors are estimated to be less than $\pm 1 \mu\text{m}$.

Figure 1(c) shows a sketch of the experimental setup. The sample is held over a printed circuit board by use of screws and nuts. Its bottom surface is in contact with a piezoelectric ceramic transducer (PZT) that acts as a source of vibrations. We use a MEGGIT Pz27 (Navy II) soft relaxor-type PZT, whose fundamental resonance frequency is 5 MHz, to cover the whole frequency range of interest. Pz27 is a soft PZT material with large coupling factor, high Curie temperature, and low mechanical quality factor. We avoid resonance effects in the transducer by working below its fundamental resonance frequency. The transformed vertical-displacement vibration signal is transmitted to the sample through a contacting screw.

We design the chain of resonators by omitting the etching of selected holes, as shown in Fig. 1(d). We purposely choose the sequence of defects to follow a rather arbitrary path in the plane of the surface, with the intent of showing that the coupling of resonators allows the tunneling of elastic waves without the creation of straight channels. The resonators are separated by $(\pm 2, \pm 1)$ or $(\pm 1, \pm 2)$ lattice shifts; that is, their absolute separation distance is fixed by the direction of the chain jumps from resonator to resonator. To verify the precision of the fabrication, an optical microscope (Leica model DM8000) is used to check the dimensions of the fabricated structures,

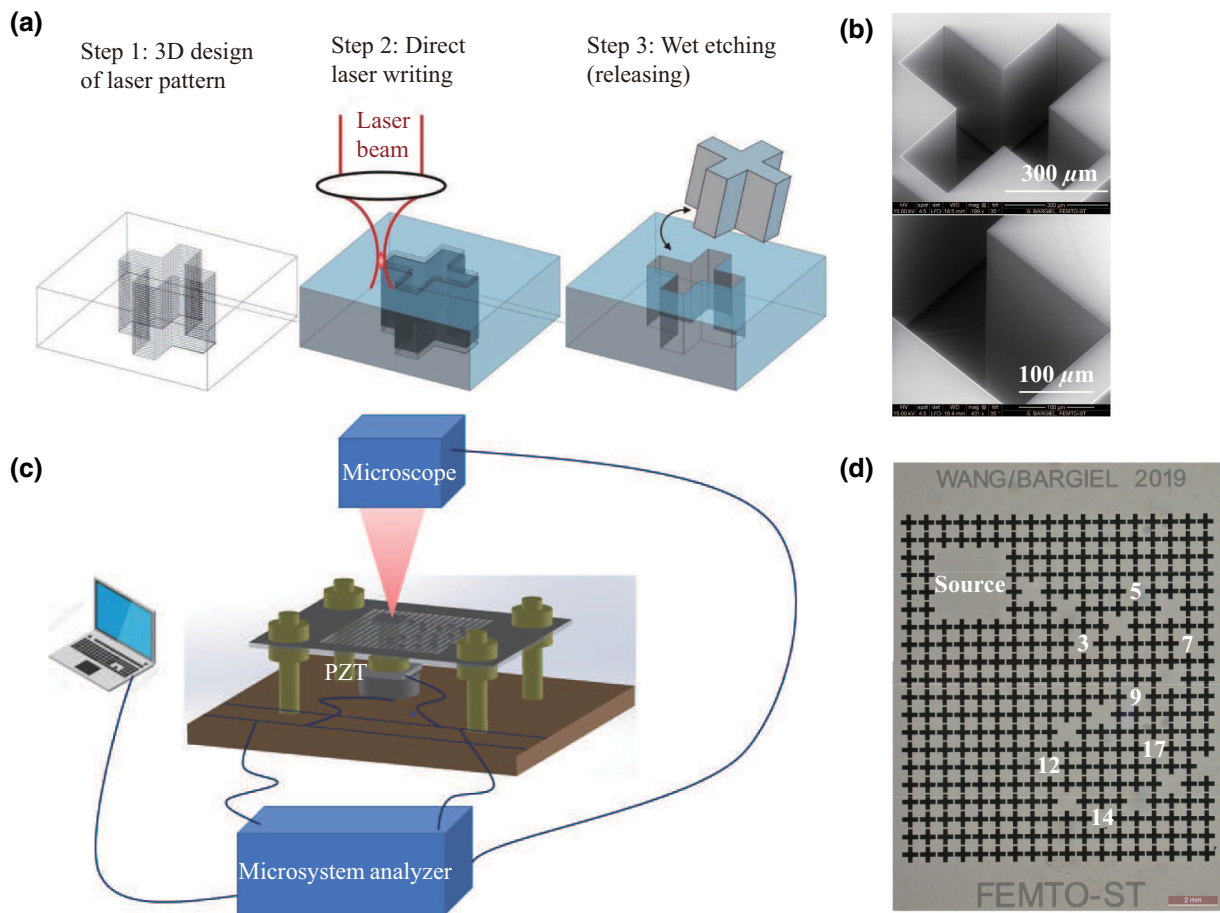


FIG. 1. Experimental setup for excitation and imaging of the vibrations of a chain of coupled resonators in a phononic crystal slab. (a) An array of cross holes forming a square lattice is etched in a fused-silica plate by femtosecond-laser-assisted wet etching. (b) A scanning-electron-microscope image of a single cross hole and an enlarged view at a sidewall, illustrating the fabrication roughness. (c) The experimental setup showing the fused-silica sample attached to a printed circuit board by screws and nuts. The bottom surface is in contact with a piezoelectric patch (PZT) acting as a source of vibrations. Out-of-plane vibrations are detected at the top surface with a laser microsystem analyzer. (d) Optical microscope image of the sample showing the chain of 17 coupled resonators embedded in a 20×18 phononic crystal of cross holes and the position of the source of vibrations.

as shown in Fig. 1(d). The resonators along the chain are numbered in sequence. The source region is placed inside the phononic crystal. For frequencies inside the complete phononic band gap, this ensures that the source region is isolated from the frame surrounding the phononic crystal structure. Evanescent coupling decreases very fast with distance, resulting effectively in near-neighbor coupling along the chain. Since the first resonator is the only one close to the source region, it is the only resonator that is significantly coupled with it.

Measurements of vibrations of the chain are conducted with a laser Doppler vibrometer (Polytec MSA-500 microsystem analyzer, equipped with analog displacement decoder model DD-300; frequency response of 0.03–24 MHz and sensitivity of 50 nm/V). A periodic chirp is chosen as the source waveform to cover the frequency range of interest. The electric signal is transformed

to a displacement vibration signal via the PZT. The vertical-displacement, or out-of-plane-displacement, signal is recorded by the vibrometer at the top surface of the sample.

All numerical simulations in this work are done by the finite-element method in three dimensions. The mechanical material parameters used for isotropic fused silica are mass density $\rho = 2201 \text{ kg/m}^3$, Poisson's ratio $\nu = 0.17$, and Young's modulus $E = 72.5 \text{ GPa}$. A 3D finite-element model is used for comparison with vibration experiments. The mesh encompasses the full 20×18 phononic crystal of cross holes, the chain of resonators, and the source. To minimize wave reflections at the lateral boundaries of the mesh, radiation boundary conditions are applied. To allow a direct comparison with experiments, a time-harmonic and spatially random wave source of vertical polarization is applied at the source region [32]. With this

setting, all possible modes of vibration are excited as the frequency is swept through the band-gap range. The frequency response function (FRF) can be recorded at any position along the sample surface. Dispersion relations and phononic band structures are obtained by our solving an eigenvalue problem with periodic boundary conditions applied at the external boundaries of the unit cell or supercell. The phononic crystal slab has a complete band gap extending from 1.5 to 4 MHz. Material loss can be estimated with the Qf factor (product of quality factor and operating frequency in hertz). $Qf \approx 5 \times 10^{12}$ for fused silica [3]. With the largest frequency considered being 4 MHz, we then have in principle $Q > 1.25 \times 10^6$ for the material loss limit. Given our experimental resolution, such fine line width cannot be resolved in practice. As a result, material damping is not added to the numerical simulations. However, radiation damping, resulting from the finite number of phononic crystal rows around the resonator chain is taken into account through the use of radiation boundary conditions.

III. RESULTS

The experimental measurement of the FRF is presented in Fig. 2(a). The line colors represent the FRF measured at different resonators. The FRF shows a series of sharp resonances within the complete phononic band gap, corresponding to vibration modes of the sample. In the following, we consider particularly the frequency regions around 2.26, 2.53, and 3.55 MHz, where the clearest signals are observed. On closer inspection, it is observed that each main response subdivides into a series of closely spaced sharp resonances, as shown in Fig. 2(c). The number of subpeaks is on the order of 18 in each case; that is, a number related to the number of coupled resonators in the chain. A similar observation was made previously regarding the channeled transmission spectrum of sonic crystal waveguides [33]. The maximum amplitude of the vertical displacement of each resonance peak varies notably, indicating that vibration modes are variously matched to the excitation source. The vertical motion at the source location is shown in Fig. 2(e) for comparison. It can be observed that the resonance peaks measured at the location of the source do not match those measured inside the chain of resonators. This is expected, since at the location of the source thickness resonances [34] of the fused-silica plate should be excited and these have a different dispersion spectrum compared with the resonators. Even when the source region vibrates very slightly, the vibrations of the chain of resonators can still be excited until the very last resonator.

The experimental results can be compared with the numerical results shown in Figs. 2(b) and 2(d). In the three frequency regions around 2.26, 2.53, and 3.55 MHz, series

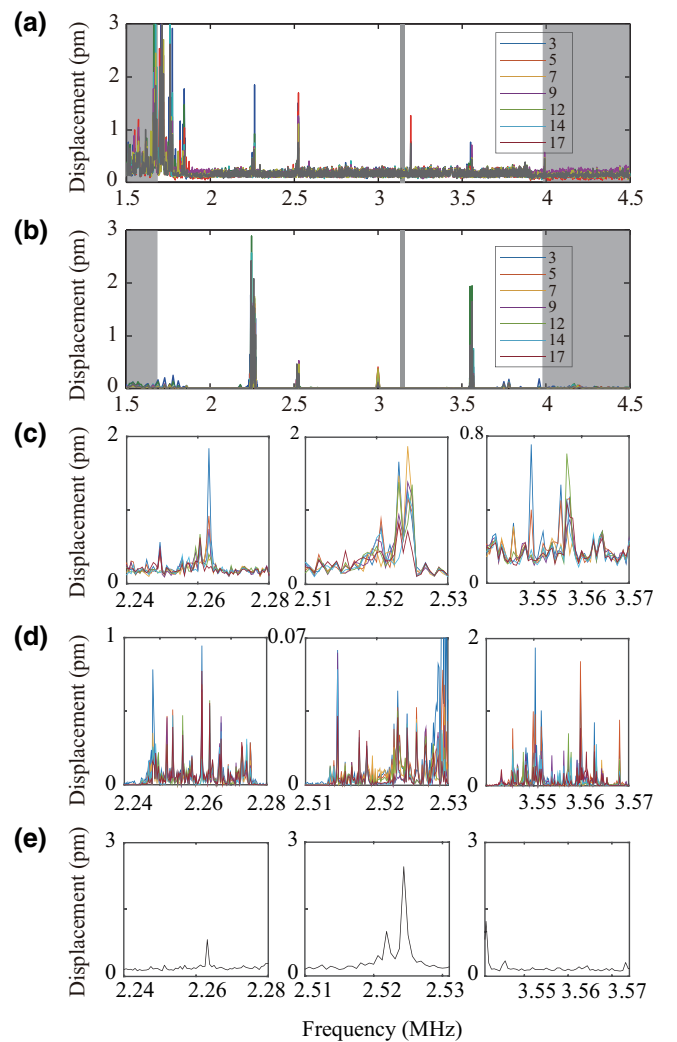


FIG. 2. (a) Experimental and (b) numerical absolute vertical displacements at the position of the resonators. Each line color is for a particular resonator as labeled in Fig. 1(b). The complete band gap extends over the white region. (c),(d) Enlarged views around selected frequencies. (e) Absolute experimental vertical displacements at the location of the source of vibrations are shown for comparison.

of sharp resonances are obtained with a frequency spacing in fair agreement with the experimental results. The experimental frequency resolution is limited to 1.56 kHz due to a limitation on the number of sample points, while numerical computations are presented with a resolution of 0.2 kHz to ensure that each peak is resolved. Generally, the numerical and experimental results agree fairly well, except for frequencies around 3 MHz, where a non zero FRF is observed only in the numerical simulation. We attribute this small discrepancy to the actual experimental environment, which differs from the numerical excitation source: the experimental excitation is not truly spatially random as is assumed in the numerical simulation. Furthermore, it may be that the excited vibrations have too small

an amplitude to be observed over the experimental noise floor.

Figure 3 displays the displacement maps observed at selected frequencies in both experiments and simulations. Animations of the vertical-displacement distribution at frequencies of 2.2625, 2.5234, and 3.5578 MHz are further shown in Videos 1, 2, and 3. It is verified that all resonators oscillate collectively at the same frequency. In all cases, vibrations are concentrated mainly at the four corners of

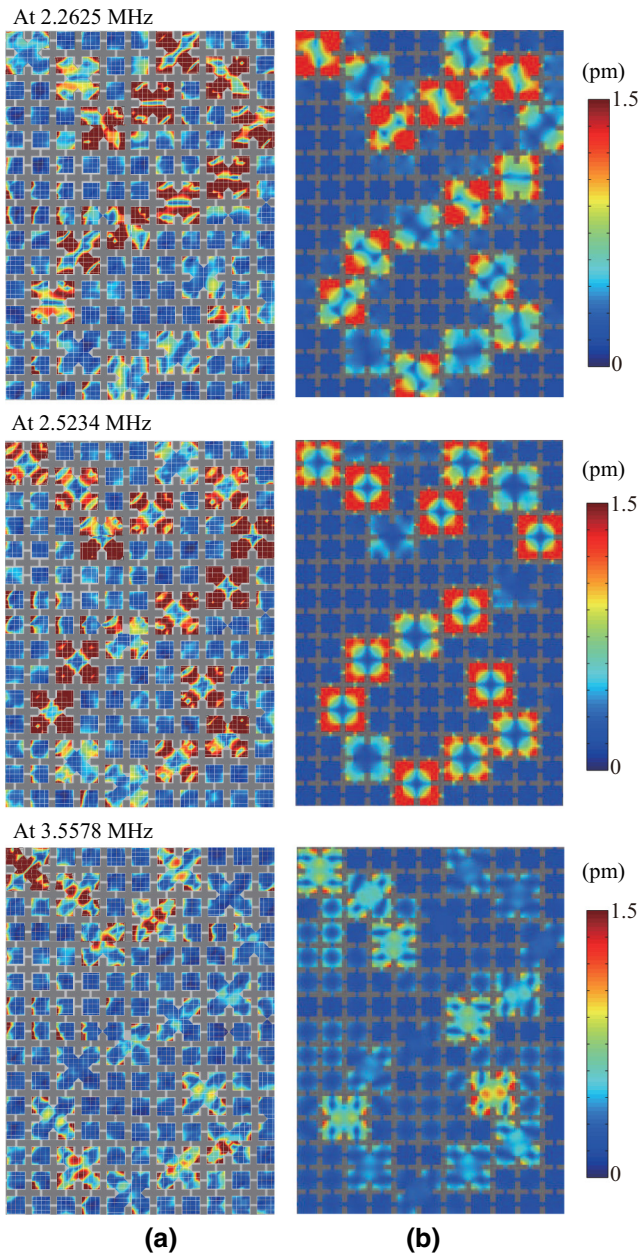
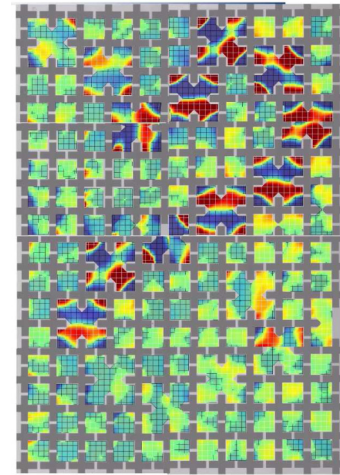


FIG. 3. Vertical-displacement maps at frequencies of 2.2625, 2.5234, and 3.5578 MHz in the experiment (a) and the numerical simulation (b), respectively. The color scale is for the amplitude of the vertical displacement from 0 (blue) to maximum (red). Numerical values are globally scaled to experimental values.



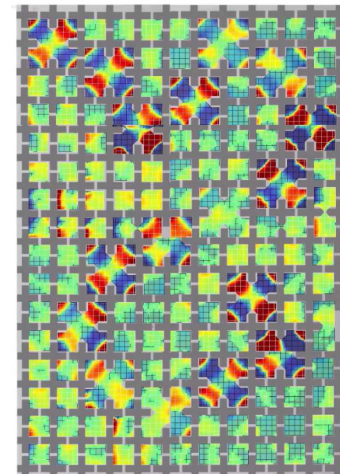
VIDEO 1. Animation of the experimental vertical-displacement distribution at a frequency of 2.2625 MHz.

the resonators. A clear modal shape repeats for every resonator, in correspondence with the initial vibration mode of the resonator. The collective vibrations are for the whole chain of resonators, without apparent spatial attenuation along the chain, and are limited only by the experimental size of the array.

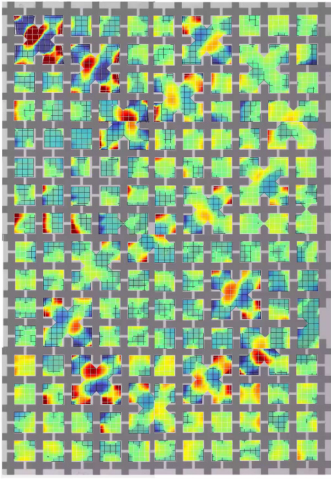
IV. MODEL OF THE PHONONIC POLYMER

A. Discrete sequence of eigenfrequencies

The chain of coupled resonators forming a phononic polymer can be analyzed with various discrete models. Hamiltonian models have been proposed, especially in the context of topological phononics [35–37]. Following the



VIDEO 2. Animation of the experimental vertical-displacement distribution at a frequency of 2.5234 MHz.



VIDEO 3. Animation of the experimental vertical-displacement distribution at a frequency of 3.5578 MHz.

Su-Schrieffer-Heeger model of polyacetylene [38], a coupling Hamiltonian can be constructed for eigenstates combining the degrees of freedom describing each resonator. Solving for the Schrödinger equation with the coupling Hamiltonian gives the sequence of eigenfrequencies. Such a technique parallels the dynamical matrix approach used to describe the dispersion of phonons in atomic lattices. Here we consider a classical version of such quantum techniques [39] where the state of the phononic polymer is described by one macroscopic degree of freedom per resonator, U_n . All resonators are identical except for a spatial shift in the crystal and have the same isolated resonance frequency ω_0 . By “isolated resonator” we mean a resonator embedded in the infinite crystal and placed very far from any other resonator.

The dynamical equation for coupled resonators is

$$-\ddot{U}_m = \sum_{n=1}^N D(m, n) U_n, \quad (1)$$

with a symmetric dynamical matrix $D(m, n)$ such that $D(m, m) = \omega_0^2$. The symmetry of the dynamical matrix is a consequence of reciprocity. For time-harmonic vibrations at a frequency ω , the dynamical equation leads to eigenfrequencies that are eigenvalues of the dynamical matrix:

$$\omega^2 U_m = \sum_{n=1}^N D(m, n) U_n. \quad (2)$$

As a result, there are exactly N eigenstates of vibration of the phononic polymer. The symmetry of the dynamical matrix implies that the eigenfrequencies ($\omega_i, i = 1 \dots N$) are real. This is the most-general form we can obtain without making further simplifying assumptions.

If the resonators are distributed evenly along the chain, it can be assumed that the dynamical matrix is banded [i.e., $D(m, n) = \gamma_{|m-n|}$], reflecting the idea of a translationally invariant chain. The coefficients $\gamma_{|m-n|}$ account for nearest-neighbor coupling. This particular assumption is made for coupled-resonator waveguides formed of an infinite chain of coupled resonators [40]. The dispersion relation for Bloch waves of the infinite periodic chain is then obtained as [39]

$$\omega^2 = 2 \sum_{m=0}^{\infty} \gamma_m \cos km\Delta. \quad (3)$$

We stress that this formula applies to the phononic polymer only in the limit $N \rightarrow \infty$.

If we further assume that only nearest-neighbor coupling occurs, then the dynamical matrix simplifies to

$$D = \begin{pmatrix} \omega_0^2 & \gamma & 0 & \cdots & 0 \\ \gamma & \ddots & \ddots & \ddots & \vdots \\ 0 & \ddots & \ddots & \ddots & 0 \\ \vdots & \ddots & \ddots & \ddots & \gamma \\ 0 & \cdots & 0 & \gamma & \omega_0^2 \end{pmatrix}. \quad (4)$$

For this particular case, the eigenfrequencies can be obtained analytically and are

$$\omega_{N,m}^2 = \omega_0^2 + 2\gamma \cos\left(\frac{\pi m}{N+1}\right), \quad m = 1 \dots N. \quad (5)$$

This result is derived in Appendix A, where it is shown that a sequence of orthogonal polynomials is formed, whose zeros are the eigenfrequencies. As a consequence, the eigenfrequencies of polymer chains with increasing number of resonators are interleaved. It is further obtained that they distribute on the continuous dispersion relation for the infinite polymer:

$$\omega^2 = \omega_0^2 + 2\gamma \cos k\Delta, \quad (6)$$

where Δ is the period of the chain and with wave number being sampled according to $k\Delta = \pi m/N + 1, m = 1 \dots N$. This condition is equivalent to the phase-matching condition introduced to describe the channeled spectrum of the transmission of phononic crystal waveguides [33]. As a generalization, we infer that if the dispersion relation $\omega^2(k\Delta)$ is known, then the resonance frequencies will be given by $\omega^2(\pi m/N + 1), m = 1 \dots N$. This distribution explains the sequence of subpeaks in Fig. 2 around each initial defect resonance.

B. Comparison with a coupled-resonator waveguide

Direct comparison of the discrete phononic polymer model with a coupled-resonator waveguide is not strictly

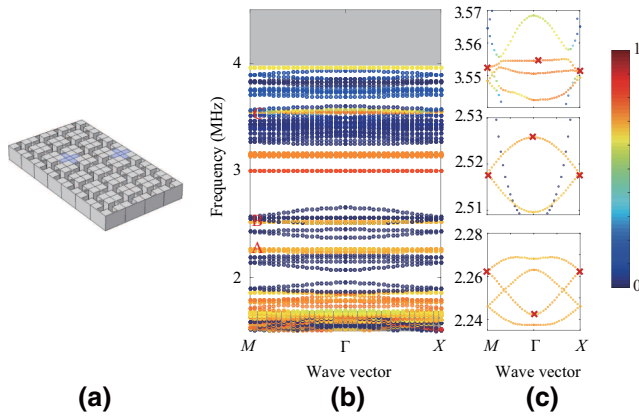


FIG. 4. Dispersion of an equivalent coupled-resonator elastic waveguide. Supercell (a), band structure (b), and enlarged band structures (c) around 2.26, 2.52, and 3.55 MHz, corresponding to points A , B , and C , respectively. Blue (red) corresponds to zero (maximum) amplitude for the out-of-plane-displacement field. The gray areas indicate the passing frequency ranges.

possible since the former is aperiodic, while the latter is periodic. Anyway, to enable comparison to some extent, we consider a simplified periodic version of the phononic polymer, as depicted by the supercell in Fig. 4(a). Compared with the actual chain of coupled resonators considered in experiments, the coupled-resonator waveguide in Fig. 4(a) implements a sequence of lattice translations $(2, -1)$ then $(2, +1)$ so that the spatial period along the x axis is $4a$ (four crosses along the x axis in the supercell). The coupled-resonator waveguide thus defined can be obtained by a continuous deformation of the chain of resonators.

Figure 4(b) shows the phononic band structure for the coupled-resonator waveguide whose supercell is presented in Fig. 4(a). The color bar indicates the polarization amount of the vertical component of displacement. Compared with the phononic band structure of the perfect crystal, additional bands appear inside the complete band gap. Figure 4(c) shows enlarged views of the band structure around 2.26, 2.52, and 3.55 MHz, corresponding to labels A , B , and C in Fig. 4(b). As a note, the $4a$ period causes spurious folding at the X and M points of the first Brillouin zone, since two periods of the chain are actually included in the supercell. As a result, there are bands in spectral ranges A and B, and presumably more in spectral range C. These bands have different polarization contents and thus couple differently with the source of vibrations. In particular, the mostly vertically polarized band in spectral range B has the cosine shape of Eq. (6), in correspondence with the single coupling coefficient of the dynamical matrix in Eq. (4). The other bands do not have this simple cosine shape, and more coupling coefficients should be included to describe them. Significantly, all bands extend almost symmetrically toward the X point and the M point, indicating that the coupling coefficients are

here mostly independent of the direction of the coupling, as we implicitly assume in the discrete model.

Eigenmodes at the high-symmetry points of the Brillouin zone on three selected bands of spectral ranges A, B, and C are illustrated in Fig. 5. It can be seen that the eigenmodes in spectral range B are identical for all high-symmetry points. We further verify that they are identical with the defect mode of the isolated resonator. More significantly, the modal shapes are clearly identical with those of Fig. 3, supporting the conclusion that the collective vibrations of the chain result from evanescent coupling of the individual resonators. In spectral range A, the situation is slightly more intricate, as two degenerate isolated defect modes coexist. They form two separate bands when unfolded, with a dispersion involving more than one Fourier harmonic; that is, corresponding to the general

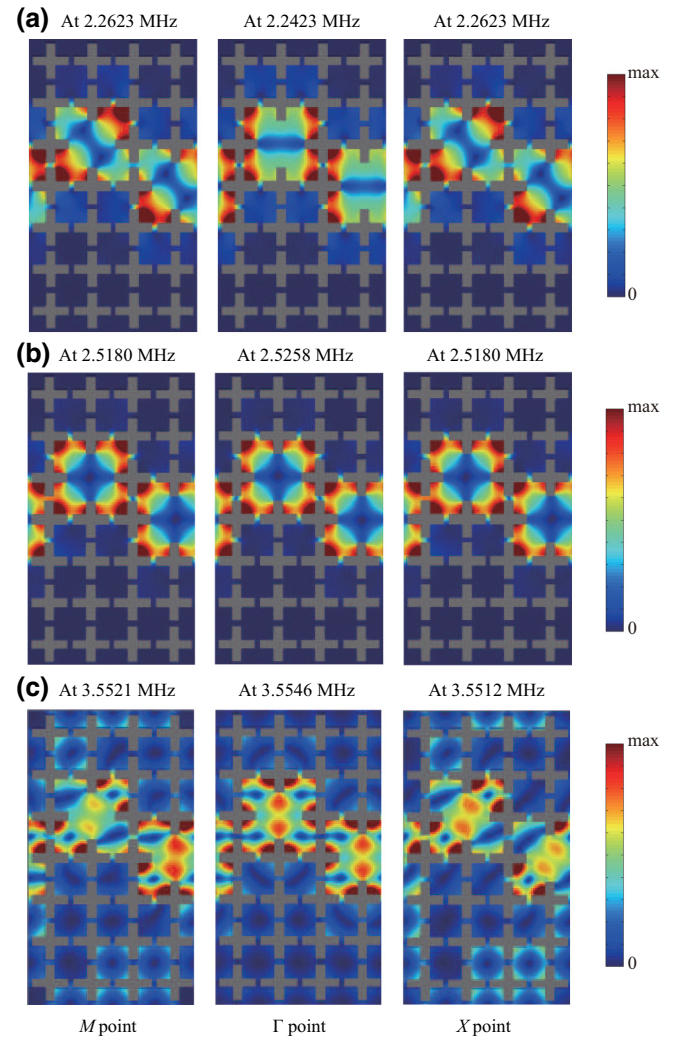


FIG. 5. Eigenmodes of the supercell shown at the M point, Γ point, and X point of the first Brillouin zone at the passing bands corresponding to A , B , and C in Fig. 4. Blue (red) corresponds to zero (maximum) amplitude for the displacement field.

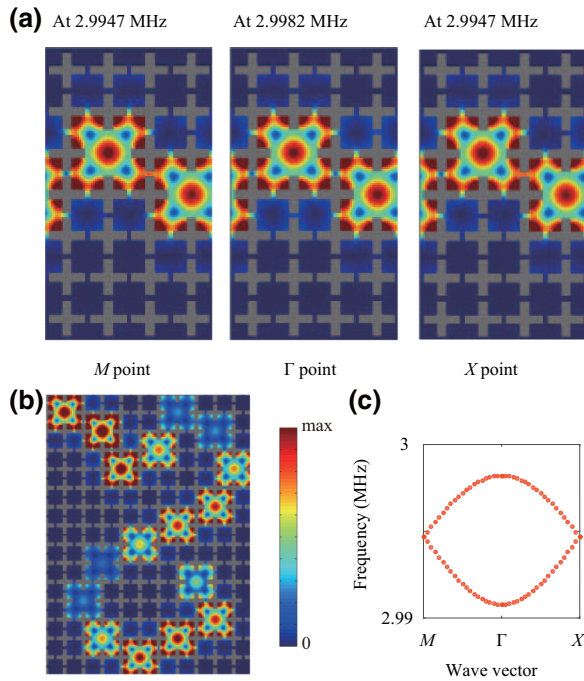


FIG. 6. Characteristics of the band appearing around 3 MHz. (a) Eigenmodes are shown at the M point, the Γ point, and the X point of the first Brillouin zone. (b) Numerical vertical-displacement map at 2.9947 MHz for the chain of resonators. (c) Band structure of the equivalent coupled-resonator elastic waveguide.

form (3) rather to the simpler form (6). In spectral range C, the bands do not have a pure out-of-plane-vibration character, and the discrete model of the phononic polymer should be enriched with up to three degrees of freedom per resonator, which we leave as a perspective.

As remarked in Sec. II, the band appearing around 3 MHz in the numerical simulation is not observed in the experiment. For completeness, however, we discuss briefly its characteristics. The eigenmodes at the M point, the Γ point, and the X point of the first Brillouin zone are shown in Fig. 6(a). These eigenmodes are identical for all three high-symmetry points. Figure 6(b) further displays the numerical displacement distribution in the chain of resonators at 3 MHz. The band in Fig. 6(c) has a cosine shape similar to the out-of-plane band in range B, indicating the dominance of nearest-neighbor coupling. Overall, the vibration characteristics at 3 MHz should be mostly similar to those at 2.5 MHz. Finally, we compare in Appendix B the acoustic transmission rate between the phononic polymer and conventional phononic waveguides with a variable number of bends.

V. CONCLUSION

In this paper, coupled elastic vibrations of a chain of coupled resonators in a square-lattice phononic crystal

slab are studied. Coupling of resonators is evanescent within the wide complete band gap obtained with cross holes, resulting in nearest-neighbor coupling. We design the chain of resonators by omitting the etching of selected holes. Measurements show that collective vibrations of the evanescently coupled resonators are efficiently excited. We image the modal vibrations over the surface and observe that the resonators oscillate collectively at the same frequency. Significantly, collective oscillations survive although the chain is aperiodic and does not form a classical phononic crystal waveguide. The number of resonances is as a rule equal to the number of resonators in the chain, in a first approximation. The evanescent-coupling mechanism we consider is indeed reminiscent of coupled-resonator waveguides. The main difference is that we do not require periodicity in the plane. This relaxed assumption allows us to design chains of resonators with a rather arbitrary shape.

This work provides a background for the consideration of phononic polymers, where resonators with equal free resonance frequency are arranged in an arbitrary chain and coupled evanescently. Active or even smart manipulation of localized resonators is thus expected. Such phononic polymers could be used for sensor-fusion purposes, with each resonator functionalized to the same or different analytes. It is expected that the collective vibrations should be highly sensitive to a local change in one of the resonators. Phononic polymers could also be used in optomechanics, using light forces such as radiation pressure to excite and detect collective resonances without any mechanical contact. Furthermore, by tuning the coupling coefficients between resonators, it should be possible to implement topological phononics models inspired, for instance, by the Su-Schrieffer-Heeger model of the polyacetylene molecule.

The fabrication process we use relies on the locally selective etching of fused silica. Other microfabrication techniques could obviously be alternatively selected in view of different material platforms or to adjust the frequency range of the ultrasonic resonances.

ACKNOWLEDGMENTS

This work was supported by the French RENATECH network and its FEMTO-ST technological facility. Financial support by the National Natural Science Foundation of China (Grants No. 11702017 and No. 11532001) is gratefully acknowledged. V.L. acknowledges financial support by the EIPHI Graduate School (Grant No. ANR-17-EURE-0002). T.-T.W. acknowledges a scholarship provided by the China Scholarship Council (Grant No. 201707090056).

APPENDIX A: SCALAR MODEL OF A CHAIN OF EQUALLY COUPLED RESONATORS

We consider of finite chain of N discrete resonators described by Eq. (4). The dynamical matrix has the form $D_N = \omega_0 I_N + \gamma C_N$, where I_N is the identity matrix of size N and

$$C_N = \begin{pmatrix} 0 & 1 & 0 & \dots & 0 \\ 1 & \ddots & \ddots & \ddots & \vdots \\ 0 & \ddots & \ddots & \ddots & 0 \\ \vdots & \ddots & \ddots & \ddots & 1 \\ 0 & \dots & 0 & 1 & 0 \end{pmatrix}. \quad (\text{A1})$$

The eigenvalues of the latter matrix are roots of the characteristic polynomial $P_N(X = \lambda) = \det(C_N - \lambda I_N)$. It is easy to check that the set of polynomials P_N thus defined satisfy the recurrence relation

$$P_{N+2} + X P_{N+1} + P_N = 0, \quad N \geq 0, \quad (\text{A2})$$

with the first two polynomials being $P_0 = 1$ and $P_1 = -X$. The next polynomials are $P_2 = X^2 - 1$, $P_3 = -X^3 + 2X$, $P_4 = X^4 - 3X^2 + 1$, and so on.

The existence of the recurrence relation (A2) implies that the set of the real polynomials P_N is orthogonal. As a consequence, their roots are all real and are interleaved. The recurrence relation resembles the one for Tchebychev polynomials, $T_{N+2} - 2X T_{N+1} + T_N = 0$. Tchebychev polynomials are characterized by the relation $T_N(\cos \theta) = \cos N\theta$ for $0 \leq \theta \leq \pi$, but are not the only set of orthogonal polynomials determined by this recurrence relation. In particular, their derivatives $U_N = (1/N)T'_N$ also are. Those polynomials satisfy $U_N(\cos \theta) = \sin N\theta / \sin \theta$ and are $U_1 = 1$, $U_2 = 2X$, $U_3 = 4X^2 - 1$, $U_4 = 8X^3 - 4X$, and so on. It is easily checked that $P_N(X) = U_{N+1}(-2X)$. The zeros of U_{N+1} are given by the condition $\sin[(N+1)\theta] / \sin \theta = 0$, or $\theta_m = m\pi / (N+1)$, $m = 1 \dots N$. As a result, the zeros of P_N are $\lambda_m = -2 \cos \theta_m = -2 \cos(m\pi / (N+1))$, $m = 1 \dots N$, and are all in the interval $[-2, 2]$.

APPENDIX B: WAVEGUIDE TRANSMISSION

The sample we prepare is designed to observe the collective vibrations of the chain of resonators, but not specifically to demonstrate waveguiding. To obtain high transmission, it would be necessary to take care of the coupling of the source with the entrance of the waveguide, but also to reduce the reflection coefficient at the exit of the chain considered as a waveguide.

To compare the acoustic transmission rate between the phononic polymer and conventional phononic waveguides, we design three additional and more-traditional coupled-resonator waveguides with a different number of bends.

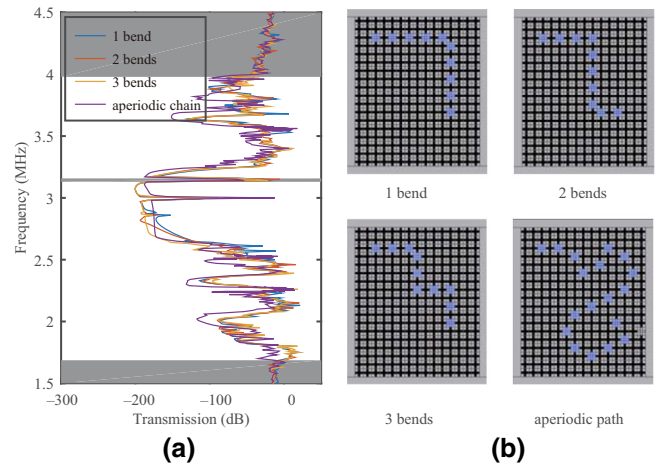


FIG. 7. (a) Transmission spectra for three circuits with a different number of bends and for the aperiodic chain. The circuits are shown in (b).

Figure 7 shows the simulated transmission spectra. We calculate the transmission rate by

$$T(fa) = \frac{\int_{S_r} U ds}{\int_{S_l} U_0 ds}, \quad (\text{B1})$$

where U is the total displacement at the exit of the waveguide and U_0 is the total displacement at the entrance of the waveguide. The main observation that we make is that the transmission spectra are similar for all waveguides and for the phononic polymer, although the details of the spectra (separation between resonances) depend on the total length of each chain. Compared with conventional coupled-resonator phononic waveguides, a distinctive advantage of the phononic polymer is that guided waves can propagate along a rather arbitrary path and not only along principal directions of the crystal.

- [1] M. S. Kushwaha, P. Halevi, L. Dobrzyński, and B. Djafari-Rouhani, Acoustic Band Structure of Periodic Elastic Composites, *Phys. Rev. Lett.* **71**, 2022 (1993).
- [2] M. M. Sigalas and E. N. Economou, Band structure of elastic waves in two dimensional systems, *Solid State Commun.* **86**, 141 (1993).
- [3] V. Laude, *Phononic Crystals: Artificial Crystals for Sonic, Acoustic, and Elastic Waves* (de Gruyter, Berlin, 2015).
- [4] V. Laude, Y. Achaoui, S. Benchabane, and A. Khelif, Evanescent Bloch waves and the complex band structure of phononic crystals, *Phys. Rev. B* **80**, 092301 (2009).
- [5] J. S. Jensen, Phononic band gaps and vibrations in one- and two-dimensional mass-spring structures, *J. Sound Vib.* **266**, 1053 (2003).

- [6] X. An, H. Fan, and C. Zhang, Elastic wave and vibration bandgaps in two-dimensional acoustic metamaterials with resonators and disorders, *Wave Motion* **80**, 69 (2018).
- [7] T.-T. Wang, Y.-F. Wang, Y.-S. Wang, and V. Laude, Evanescent-wave tuning of a locally resonant sonic crystal, *Appl. Phys. Lett.* **113**, 231901 (2018).
- [8] Y.-F. Wang, V. Laude, and Y.-S. Wang, Coupling of evanescent and propagating guided modes in locally resonant phononic crystals, *J. Phys. D: Appl. Phys.* **47**, 475502 (2014).
- [9] M. Torres, F. R. Montero de Espinosa, D. García-Pablos, and N. García, Sonic Band Gaps in Finite Elastic Media: Surface States and Localization Phenomena in Linear and Point Defects, *Phys. Rev. Lett.* **82**, 3054 (1999).
- [10] Y. Pennec, J. O. Vasseur, B. Djafari-Rouhani, L. Dobrzyński, and P. A. Deymier, Two-dimensional phononic crystals: Examples and applications, *Surf. Sci. Rep.* **65**, 229 (2010).
- [11] Y. Akahane, M. Mochizuki, T. Asano, Y. Tanaka, and S. Noda, Design of a channel drop filter by using a donortype cavity with high-quality factor in a two-dimensional photonic crystal slab, *Appl. Phys. Lett.* **82**, 1341 (2003).
- [12] T.-T. Wang, Y.-F. Wang, Y.-S. Wang, and V. Laude, Tunable fluid-filled phononic metastrip, *Appl. Phys. Lett.* **111**, 041906 (2017).
- [13] Y. Jin, N. Fernez, Y. Pennec, B. Bonello, R. P. Moiseyenko, S. Hémon, Y. Pan, and B. Djafari-Rouhani, Tunable waveguide and cavity in a phononic crystal plate by controlling whispering-gallery modes in hollow pillars, *Phys. Rev. B* **93**, 054109 (2016).
- [14] A. Yariv, Y. Xu, R. K. Lee, and A. Scherer, Coupled-resonator optical waveguide: A proposal and analysis, *Opt. Lett.* **24**, 711 (1999).
- [15] M. Notomi, E. Kuramochi, and T. Tanabe, Large-scale arrays of ultrahigh-Q coupled nanocavities, *Nat. Photonics* **2**, 741 (2008).
- [16] T. Baba, Slow light in photonic crystals, *Nat. Photonics* **2**, 465 (2008).
- [17] L. Xia, F. Sekaric, and Y. Vlasov, Ultracompact optical buffers on a silicon chip, *Nat. Photonics* **1**, 65 (2007).
- [18] J. Wang, Z. Yao, T. Lei, and A. W. Poon, Silicon coupled-resonator optical-waveguide-based biosensors using light-scattering pattern recognition with pixelized mode-field-intensity distributions, *Sci. Rep.* **4**, 7528 (2014).
- [19] C. R. Otey, M. L. Povinelli, and S. Fan, Completely capturing light pulses in a few dynamically tuned microcavities, *J. Lightwave Technol.* **26**, 3784 (2008).
- [20] R. F. Oulton, V. J. Sorger, D. A. Genov, D. F. P. Pile, and X. Zhang, A hybrid plasmonic waveguide for sub-wavelength confinement and long-range propagation, *Nat. Photonics* **2**, 496 (2008).
- [21] A. Khelif, A. Choujaa, S. Benchabane, B. Djafari-Rouhani, and V. Laude, Guiding and bending of acoustic waves in highly confined phononic crystal waveguides, *Appl. Phys. Lett.* **84**, 4400 (2004).
- [22] D. Hatanaka, I. Mahboob, K. Onomitsu, and H. Yamaguchi, Phonon waveguides for electromechanical circuits, *Nat. Nanotechnol.* **9**, 520 (2014).
- [23] Y.-F. Wang, T.-T. Wang, J.-P. Liu, Y.-S. Wang, and V. Laude, Guiding and splitting Lamb waves in coupled-resonator elastic waveguides, *Comput. Struct.* **206**, 588 (2018).
- [24] Y.-F. Wang, T.-T. Wang, Y.-S. Wang, and V. Laude, Reconfigurable Phononic-Crystal Circuits Formed by Coupled Acoustoelastic Resonators, *Phys. Rev. Appl.* **8**, 014006 (2017).
- [25] I. E. Psarobas, N. Stefanou, and A. Modinos, Phononic crystals with planar defects, *Phys. Rev. B* **62**, 5536 (2000).
- [26] A. Khelif, A. Choujaa, B. Djafari-Rouhani, M. Wilm, S. Ballandras, and V. Laude, Trapping and guiding of acoustic waves by defect modes in a full-band-gap ultrasonic crystal, *Phys. Rev. B* **68**, 214301 (2003).
- [27] Y. Pennec, B. Djafari-Rouhani, J. O. Vasseur, H. Larabi, A. Khelif, A. Choujaa, S. Benchabane, and V. Laude, Acoustic channel drop tunneling in a phononic crystal, *Appl. Phys. Lett.* **87**, 261912 (2005).
- [28] S. Benchabane, R. Salut, O. Gaiffe, V. Soumann, M. Addouche, V. Laude, and A. Khelif, Surface-Wave Coupling to Single Phononic Subwavelength Resonators, *Phys. Rev. Appl.* **8**, 034016 (2017).
- [29] L. Raguin, O. Gaiffe, R. Salut, J.-M. Cote, V. Soumann, V. Laude, A. Khelif, and S. Benchabane, Coherent interplay between surface acoustic waves and coupled mechanical resonators: Transition from plasmon-like to surface mediated coupling, *Nat. Commun.* **10**, 4583 (2019).
- [30] Y. Bellouard, A. Said, M. Dugan, and P. Bado, Fabrication of high-aspect ratio, micro-fluidic channels and tunnels using femtosecond laser pulses and chemical etching, *Opt. Express* **12**, 2120 (2004).
- [31] Audrey Champion and Yves Bellouard, Direct volume variation measurements in fused silica specimens exposed to femtosecond laser, *Opt. Mat. Express* **2**, 789 (2012).
- [32] V. Laude and M. E. Korotyaeva, Stochastic excitation method for calculating the resolvent band structure of periodic media and waveguides, *Phys. Rev. B* **97**, 224110 (2018).
- [33] Y.-F. Wang, T.-T. Wang, J.-W. Liang, Y.-S. Wang, and V. Laude, Channeled spectrum in the transmission of phononic crystal waveguides, *J. Sound Vib.* **437**, 410 (2018).
- [34] Thickness resonances are standing Lamb waves of the homogeneous plate, having a zero lateral wave number.
- [35] P. Wang, L. Lu, and K. Bertoldi, Topological Phononic Crystals with One-Way Elastic Edge Waves, *Phys. Rev. Lett.* **115**, 104302 (2015).
- [36] S. H. Mousavi, A. B. Khanikaev, and Z. Wang, Topologically protected elastic waves in phononic metamaterials, *Nat. Commun.* **6**, 8682 (2015).
- [37] R. Süssstrunk and S. D. Huber, Observation of phononic helical edge states in a mechanical topological insulator, *Science* **349**, 47 (2015).
- [38] W. P. Su, J. R. Schrieffer, and A. J. Heeger, Solitons in Polyacetylene, *Phys. Rev. Lett.* **42**, 1698 (1979).
- [39] Jose Maria Escalante, Alejandro Martínez, and Vincent Laude, Dispersion relation of coupled-resonator acoustic waveguides formed by defect cavities in a phononic crystal, *J. Phys. D: Appl. Phys.* **46**, 475301 (2013).
- [40] For a finite chain of coupled resonators, there are in principle end effects that break the banded-matrix assumption: resonators at either end do not see the same environment as resonators in the middle of the chain.